SCIENTIFIC COMMUNICATIONS

MAPPING HYDROTHERMALLY ALTERED ROCKS AT CUPRITE, NEVADA, USING THE ADVANCED SPACEBORNE THERMAL EMISSION AND REFLECTION RADIOMETER (ASTER), A NEW SATELLITE-IMAGING SYSTEM

LAWRENCE C. ROWAN,[†]

U.S. Geological Survey, Mail Stop-954, Reston, Virginia 20192

SIMON J. HOOK, MICHAEL J. ABRAMS,

Jet Propulsion Laboratory, 4800 Oak Grove Drive, Pasadena, California 91109-8099

AND JOHN C. MARS

U.S. Geological Survey, Mail Stop-954, Reston, Virginia 20192

Abstract

The Advanced Spaceborne Thermal Emission and Reflection Radiometer (ASTER) is a 14-band multispectral instrument on board the Earth Observing System (EOS), TERRA. The three bands between 0.52 and 0.86 μm and the six bands from 1.60 and 2.43 μm, which have 15- and 30-m spatial resolution, respectively, were selected primarily for making remote mineralogical determinations.

The Cuprite, Nevada, mining district comprises two hydrothermal alteration centers where Tertiary volcanic rocks have been hydrothermally altered mainly to bleached silicified rocks and opalized rocks, with a marginal zone of limonitic argillized rocks. Country rocks are mainly Cambrian phyllitic siltstone and limestone.

Evaluation of an ASTER image of the Cuprite district shows that spectral reflectance differences in the nine bands in the 0.52 to 2.43 μm region provide a basis for identifying and mapping mineralogical components which characterize the main hydrothermal alteration zones: opal is the spectrally dominant mineral in the silicified zone; whereas, alunite and kaolinite are dominant in the opalized zone. In addition, the distribution of unaltered country rocks was mapped because of the presence of spectrally dominant muscovite in the siltstone and calcite in limestone, and the tuffaceous rocks and playa deposits were distinguishable due to their relatively flat spectra and weak absorption features at 2.33 and 2.20 μm, respectively.

An Airborne Visible/Infrared Imaging Spectrometer (AVIRIS) image of the study area was processed using a similar methodology used with the ASTER data. Comparison of the ASTER and AVIRIS results shows that the results are generally similar, but the higher spectral resolution of AVIRIS (224 bands) permits identification of more individual minerals, including certain polymorphs. However, ASTER has recorded images of more than 90 percent of the Earth's land surface with less than 20 percent cloud cover, and these data are available at nominal or no cost. Landsat TM images have a similar spatial resolution to ASTER images, but TM has fewer bands, which limits its usefulness for making mineral determinations.

Introduction

The development of methods for mapping rock types has been one of the main goals of geological remote sensing research. Hydrothermally altered rocks have received considerable attention because of their potential economic implications and favorable spectral characteristics for remote identification (Rowan et al., 1974, 1977; Abrams et al., 1977, 1983; Goetz et al, 1983; Podwysocki et al., 1983; Kruse et al., 1993; Swayze et al., 1998; among others). The Cuprite, Nevada, mining district has served as a test site for numerous experiments designed to evaluate and improve remote sensing instruments for identifying and mapping lithologic units. The earliest experiment, conducted during 1976 using the Bendix 24-channel airborne scanner, was designed to evaluate the usefulness of spectral bands positioned in the shortwave-infrared (SWIR) region (1.0 to 2.5 μm) for mapping the bleached, limonite-deficient hydrothermally altered rocks

which are very well exposed in two acid-sulfate hydrothermal alteration centers (Abrams et al., 1977). The success of that study was critical to the 1978 decision to place the seventh band in the Landsat Thematic Mapper (TM) in the 2.2-μm region. Subsequent research in the district has been focused on the use of high spectral resolution imaging systems, such as the Airborne Visible/Infrared Imaging Spectrometer (AVIRIS), to identify individual minerals and to map their distribution (Goetz and Srivastava, 1985; Kruse et al., 1990; Rast et al., 1991; Hook et al., 1991; Swayze, 1997; Swayze et al., 1992, 1998).

The purpose of this communication is to describe the capability of the Advanced Spaceborne Thermal Emission and Reflection Radiometer (ASTER) for mapping the hydrothermally altered rocks and the country rocks in the Cuprite mining district. The ASTER instrument is included on the Earth Observing System (EOS) TERRA platform, which was launched in December 1999, and records radiation from the Earth in 14 spectral bands (Fig. 1, Table 1). ASTER measures
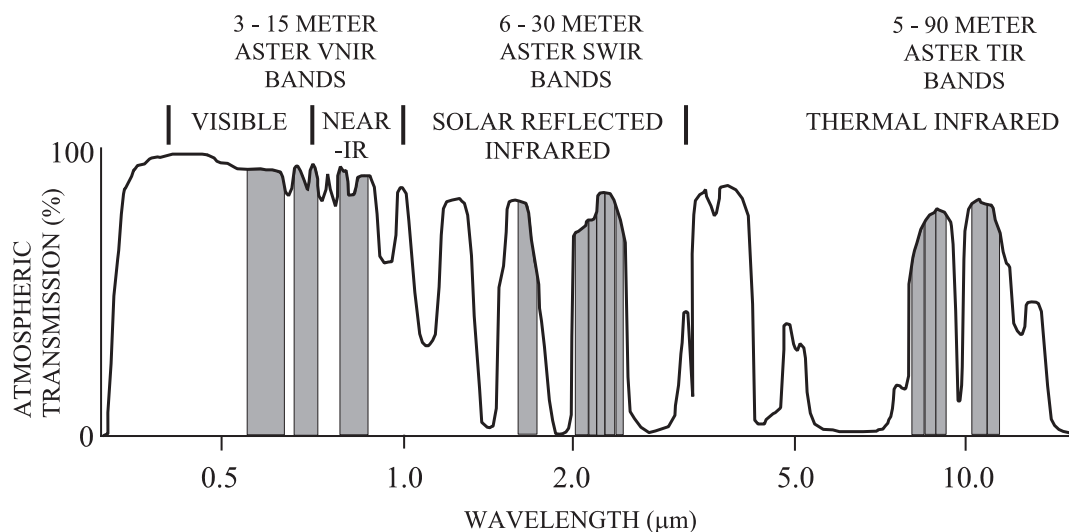
FIG. 1. Generalized atmospheric transmission spectrum showing the location of ASTER spectral bands in the absorption windows.

TABLE 1. Performance Parameters for the ASTER Radiometer (Fujisada, 1995)

ASTER baseline performance requirements

Spectrometer	Band no.	Bandpass (spectral range) (μm)	Radiometric resolution	Absolute accuracy [1] (σ)	Spatial resolution (m)	Signal quantization levels [2] (bits)
VNIR	1	0.52–0.60	NE$\Delta\rho$ ≤0.5 %	≤±4%	15	8
	2	0.63–0.69	NE$\Delta\rho$ ≤0.5 %	≤±4%	15	8
	3N	0.78–0.86	NE$\Delta\rho$ ≤0.5 %	≤±4%	15	8
	3B	0.78–0.86	NE$\Delta\rho$ ≤0.5 %	≤±4%	15	8
SWIR	4	1.600–1.700	NE$\Delta\rho$ ≤0.5 %	≤±4%	30	8
	5	2.145–2.185	NE$\Delta\rho$ ≤1.3 %	≤±4%	30	8
	6	2.185–2.225	NE$\Delta\rho$ ≤1.3 %	≤±4%	30	8
	7	2.235–2.285	NE$\Delta\rho$ ≤1.3 %	≤±4%	30	8
	8	2.295–2.365	NE$\Delta\rho$ ≤1.0 %	≤±4%	30	8
	9	2.360–2.430	NE$\Delta\rho$ ≤1.3 %	≤±4%	30	8
TIR	10	8.125–8.475	NEΔT ≤0.3 %	≤±4%	90	12
	11	8.475–8.825	NEΔT ≤0.3 %	≤3k (200–240)	90	12
	12	8.925–9.275	NEΔT ≤0.3 %	≤2k (240–270)	90	12
	13	10.25–10.95	NEΔT ≤0.3 %	≤1k (270–340)	90	12
	14	10.95–11.65	NEΔT ≤0.3 %	≤2k (340–370)	90	12

Stereo base-to-height ratio	0.6 (along-track)
Swath width	60 km
Total coverage in cross-track direction by pointing	232 km, VNIR = ±24 °, SWIR AND TIR = ±8.55°
Mission life	5 yr
MTF at Nyquist frequency [3]	0.25 (cross-track), 0.20 (along-track)
Band-to-band registration [4]	Intra-telescope: 0.2 pixels
	Inter-telescope: 0.3 pixels of coarser band
Peak data rate	89.2 mpbs
Mass	406 kg
Peak power	726 W

Noise Equivalent Delta Reflectance (NE$\Delta\rho$) refers to absolute radiometric accuracy in the VNIR and SWIR bands, and noise equivalent delta temperature (NEΔT) refers to absolute temperature accuracy in the TIR bands

[1] Absolute radiometric accuracy = conformity of radiance measurement to value at standard target
[2] Signal quantization level = digitization level of measured radiance
[3] MTF of Nyquist frequency = function which measures the spatial frequency modulation response at one-half the sampling rate
[4] Band-to-band registration = accuracy with which pixels from corresponding x, y positions at different wavelengths correspond

reflected radiation in three bands between 0.520 and 0.860 μm (visible-near-infrared region—VNIR) and in six bands from 1.00 to 2.43 μm (short-wave infrared region—SWIR), with 15-m and 30-m spatial resolution, respectively (Fujisada, 1995). Stereoscopic images can be acquired at 15-m resolution by imaging with the back-looking telescope as well as the nadir-viewing system. In addition, emitted radiation is measured in five bands in the 8.125- to 11.650-μm wavelength region (thermal-infrared region—TIR) at 90-m resolution. The swath-width is 60 km, but the pointing capability of ASTER extends the total cross-track capability to 232 km (Fujisada, 1995). The data acquisition plan was designed to record at least once a set of reasonably cloud-free images in all 14 bands, including stereoscopic coverage, of most of the land surface during ASTER's anticipated five-year lifetime. ASTER data is available from the U.S. Geological Survey EROS Data Center, Sioux Falls, S.D. (http://edcimswww.cr.usgs.gov/pub), and additional information is available at the ASTER web site (asterweb.jpl.nasa.gov). In addition, multi-temporal images are acquired to support NASA-approved investigations, and expedited coverage is provided of dynamic events, such as volcanic eruptions and floods. This study focuses on the usefulness of the VNIR and SWIR bands (1–9) for geologic mapping.

Geologic Setting

The Cuprite district is in the extreme southwestern part of the Great Basin approximately 15 km south of Goldfield, Nevada, (Fig. 2). Copper, silver, gold and lead occurrences have been reported in Cambrian limestone, and sulfur occurs in Tertiary tuffaceous sedimentary rocks and welded ash-flow tuffs (Albers and Stewart, 1972). The area is readily accessible, as it is bisected by U.S. Highway 95, and relief is low to moderate (approx 1,424 to 1,700 m asl).

The oldest rocks in the district are Cambrian sedimentary rocks, which are well exposed in the western part (Fig. 2). These include the Harkless Fm., the Mule Spring Limestone, and the Emigrant Fm. The Harkless Fm. (Єh, Fig. 2) consists mainly of greenish phyllitic siltstone, which is composed of muscovite, chlorite, biotite, and quartz (Albers and Stewart, 1972; Ashley and Abrams, 1980). Sandy limestone is exposed locally. The Mule Spring Limestone (Єms, Fig. 2) overlies the Harkless Formation and consists of gray, finely crystalline, thin-bedded limestone (Albers and Stewart, 1972; Ashley and Abrams, 1980). Brown, limey siltstone is present in the lower parts of the section. The Emigrant Formation (Єe, Fig. 2) consists of thinly bedded limestone and chert, and exposures are limited to a few small areas in the northwestern and southwestern parts of the district.

The oldest Tertiary unit (Ts, Fig. 2) includes crystal-rich rhyolite or quartz latite tuff and sedimentary and volcanic rocks exposed in the eastern part of the area, which are apparently correlative with the Siebert Tuff (Ashley and Abrams, 1980), and a quartz latitic felsite dike in the western part (Tf, Fig. 2). The Siebert Tuff consists of a lower succession of ash-flow tuffs, including coarse-grained tuff and pumice lapilli and tuff breccia, and a lower unit of volcanic conglomerate and sandstone, which Swayze (1997) refers to as Cuprite Hills Conglomerate no. 1. There are also limited exposures of porphyritic plagioclase olivine basalt flow-rock
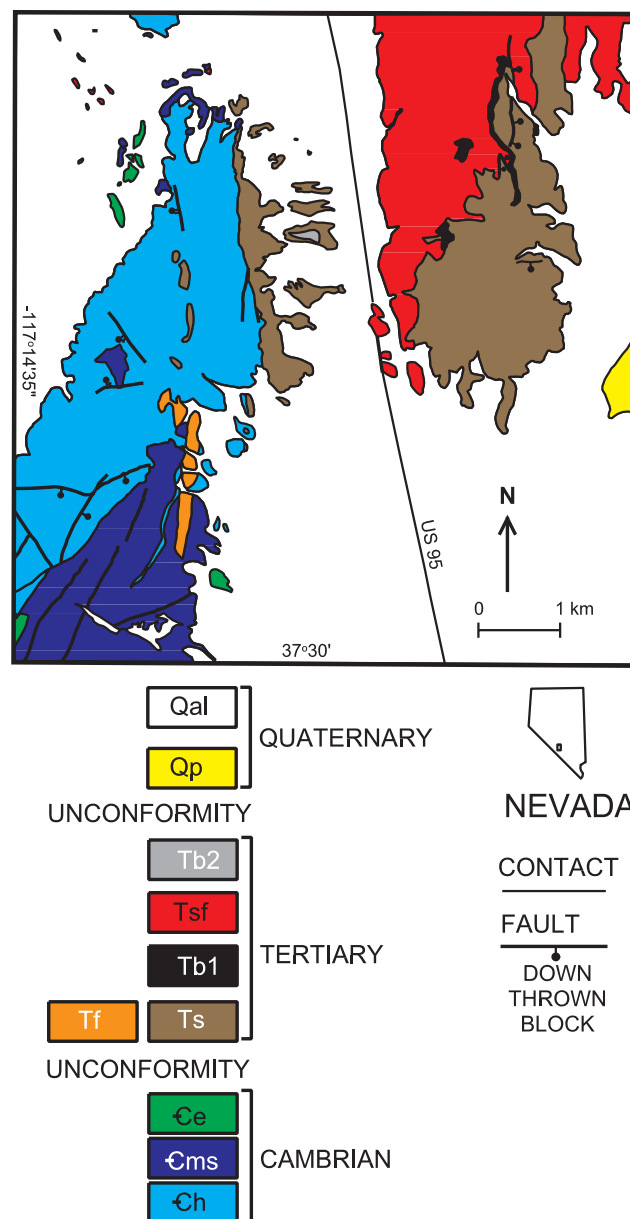

FIG. 2. Generalized geologic map of the Cuprite mining district, Nevada. Qal = sand, gravel, and boulders; Qp = playa deposits; Tb2 = olivene basalt; Tsf = sodic ash-flow tuff; Tb1 = porphyritic olivene basalt; Ts = crystal-rich rhyolite and latite tuff, conglomerate, and sandstone; Tf = quartz latitic felsite; Єe = limestone and chert; Єms = limestone and lower limey siltstone; Єh = phyllitic siltstone and minor sandy limestone (modified from Ashley and Abrams, 1980; Swayze, 1997); inset map shows location of area in western Nevada.

(Tb1, Fig. 2) in the eastern part of the area. The extensive exposures of Stonewall Flat Tuff (Tsf, Fig. 2) comprise two devitrified sodic rhyolite ash-flow tuffs, which are approximately 7.6 Ma (Ashley and Abrams, 1980; Weiss and Noble, 1989; Hausback et al., 1990; Swayze, 1997). The quartz latite dike contains alkali feldspar and biotite phenocrysts (Ashley and Abrams, 1980; Swayze et al., 1998). The Tertiary volcanic rocks are extensively altered both in the western and eastern parts of the district. The Cuprite Hills Conglomerate no. 2 of Swayze (1997) is well exposed along the lower eastern slopes

of the western center and near the ridge crest above these slopes (Fig. 2). The Pediment Basalt is limited to a single exposure, which is situated west of the highway (Tb2, Fig. 2).

Quaternary sand and gravel deposits with local concentrations of boulders cover the slopes of these well-exposed areas (Qal, Fig. 2). The playa in the southeastern part of the area (Qp, Fig. 2) is an important lithologic unit, because some of its mineral constituents are similar to those present in the hydrothermally altered rocks.

Hydrothermally Altered Rocks

Ashley and Abrams (1980) described three map units of hydrothermally altered rocks (Fig. 3), which cover approximately 12 km^2: (1) silicified, (2) opalized, and (3) argillized rock units. Silicified rocks, which are the most intensely altered and most widespread in the alteration center east of the highway, consist of hydrothermal quartz and minor calcite, kaolinite, and alunite (Ashley and Abrams, 1980). These rocks have a vuggy texture, and a dark desert varnish is present on about one-third of the outcrop surfaces.
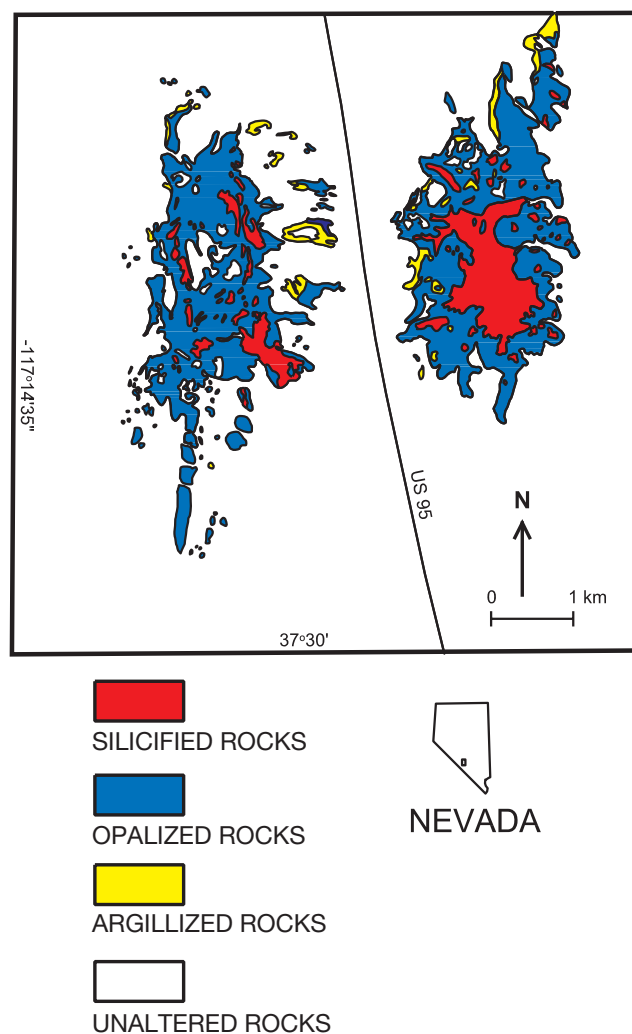

FIG. 3. Generalized map showing the distribution of three hydrothermally altered rock units: (1) red, silicified; (2) blue, opalized; and (3) yellow, argillized. Modified from Ashley and Abrams (1980).

Opalized rocks are the most widespread type of hydrothermally altered rocks, and a large variety of minerals have been recognized, including alunite, kaolinite, opal, dickite, pyrophyllite, calcite, buddingtonite, muscovite, montmorillonite, and jarosite (Ashley and Abrams, 1980; Swayze et al., 1992, 1998; Swayze, 1997). This assemblage is similar to the advanced argillic alteration described by Meyer and Hemley (1967), except that opal is more abundant in the Cuprite opalized rocks.

Argillized rocks, which are the least intensely altered rocks in the district, are confined to the margins of the alteration zone. Plagioclase is typically altered to kaolinite, biotite is bleached, and volcanic glass is altered to opal, montmorillonite, and kaolinite; primary quartz and sanadine are generally unaltered. Limonite content of most of the altered rocks is less than 5 percent, and most surfaces are nearly limonite-free (Ashley and Abrams, 1980). Limonite is relatively abundant in the argillized rocks, and in some opalized rock exposures in the western part of the district.

In the western alteration center Swayze et al. (1998) mapped areas of argillic rocks surrounding propylitic rocks. Ashley and Abrams (1980) note that weakly altered volcanic and sedimentary rocks are widespread in the district.

Spectral Reflectance

Visible and near-infrared reflectance spectra of rocks commonly display intense absorption features due to electronic processes in transition metals, such as Fe, and to molecular vibrational processes in hydroxyl- and carbonate-bearing minerals. Visible and near-infrared laboratory reflectance spectra of rock samples collected in the Cuprite district are shown in Figure 4 both at fine spectral resolution, and at ASTER resolution. The collection locations of these samples are shown in an ASTER band 1 image (Fig. 5).

The Al-O-H, Mg-O-H, CO$_3$, and Si-O-H absorption features displayed in Figure 4 are overtones and combination bands of fundamental features, which occur in the TIR wavelength region (Hunt, 1977). Spectral absorption features such as these are particularly important in the Cuprite district because of the abundance of hydroxyl-bearing minerals and the low ferric-mineral content of the hydrothermally altered rocks. They have been exploited extensively to map individual minerals by using high spectral-resolution imaging systems, particularly AVIRIS (Green, 1991) and HyMap (Cocks et al., 1998). High-spectral resolution airborne data have been used to map spatial variations by detecting subtle shifts in the wavelength position of certain absorption features (Swayze et al., 1992, 1998; Swayze, 1997).

ASTER has nine bands in the VNIR-SWIR wavelength region, so the resampled spectra of these samples lack the detail that is evident in the high-resolution laboratory spectra (Fig. 4). However, the general shapes of the different absorption features are distinctively preserved in the ASTER spectra. Note that five of the ASTER bands are concentrated in the wavelength region between 2.1 and 2.4 μm in order to measure reflectance of the spectrally diagnostic Al-O-H, Mg-O-H, CO$_3$, and Si-O-H absorption features. For comparison, the Landsat Thematic Mapper (TM) imaging system has one band in this wavelength region, which is not adequate for distinguishing among these absorption features (Goetz and others, 1983).
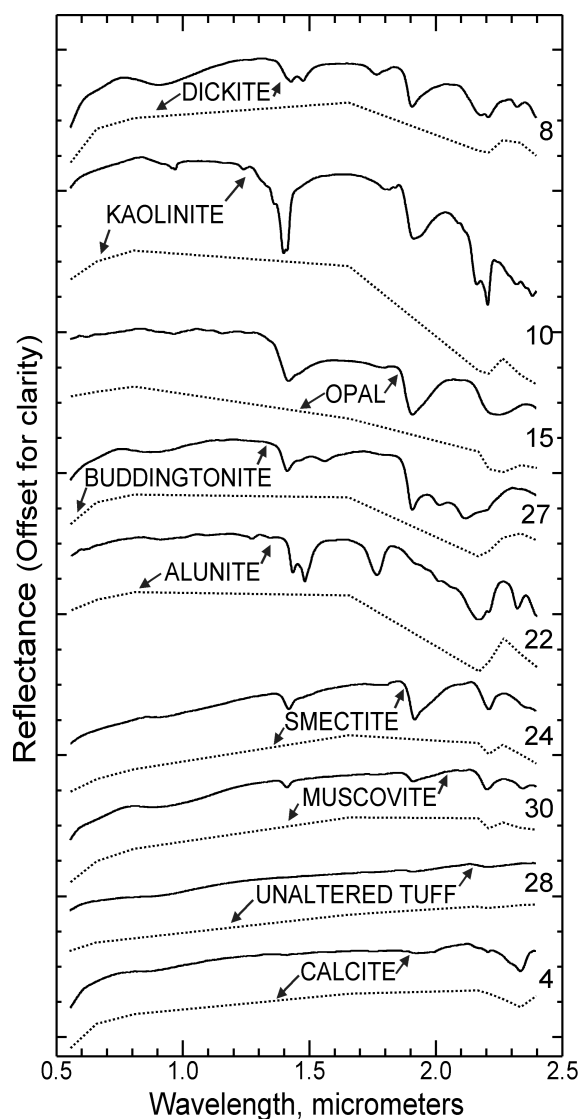
FIG. 4. Laboratory reflectance spectra of samples collected in the Cuprite district (locations shown in Fig. 5). The spectrally dominant mineral is indicated for each sample. In each pair of spectra the upper spectrum is plotted at fine spectral resolution (solid lines); whereas, the lower spectrum has been resampled to the nine ASTER VNIR-SWIR bandpasses (dashed lines).
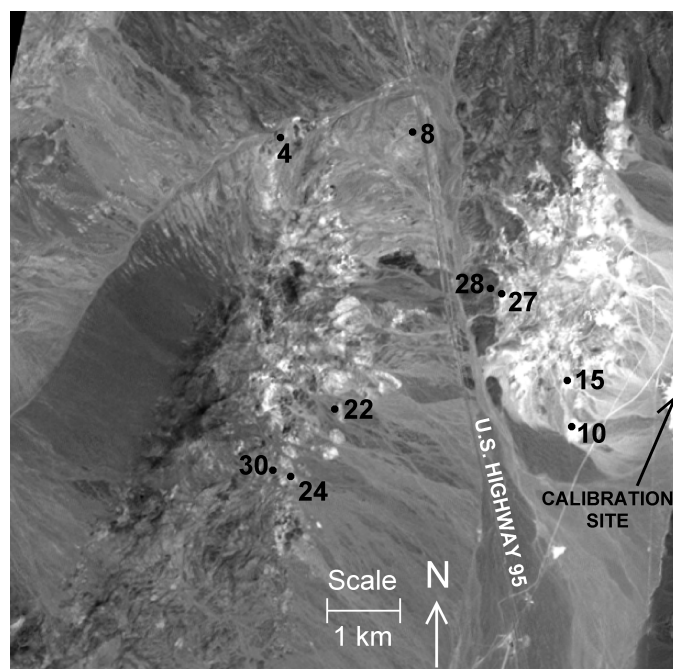

FIG. 5. ASTER band one image of the Cuprite mining district, Nevada showing the location of the samples whose spectra are plotted in Figure 4, and the location of the in situ calibration site on the playa in the southeastern part of the study area.

bands or the 224 bands of AVIRIS. Initially, the data values are so strongly modulated by the solar response function and by atmospheric absorption and scattering that the spectra do not resemble the actual reflectance of the surface materials. Calibration to minimize these influences can be accomplished by using an atmospheric model, or by reference to an object in the image for which the reflectance spectrum is known (Crowley et al., 1988; Clark et al., 1995; Rowan and Mars, 2003). In this study the ASTER image data were calibrated to spectral reflectance by reference to the average in situ spectrum measured on a part of the playa in the southeastern part of the image (Fig. 5). The AVIRIS data were calibrated previously at the Jet Propulsion Laboratory, Pasadena, California, by using a MODTRAN atmospheric radiative transfer function (Green, 1991), and are available on the AVIRIS website (http://popo.jpl.nasa.gov).

ASTER image analysis

Identification and mapping of mineralogic units or classes through spectral analysis of calibrated multispectral VNIR and SWIR images requires (1) selecting representative reflectance spectra of mineralogic classes for reference in the analysis; and (2) implementing a spectral analysis algorithm to evaluate the degree of match of each pixel's spectrum to the reference spectrum (Rowan and Mars, 2003). An effective method for locating pixels, which represent spectrally distinctive classes, is the "pixel purity index" algorithm (Boardman et al., 1995). In sparsely vegetated areas, the identified pixels tend to consist of rocks in which one or two minerals have dominant absorption features, such as those in Figure 4. The spectrally distinctive classes selected in this manner are referred to here as "spectral endmembers." An alternative

Data Processing and Analysis

A cloud-free ASTER scene of the Cuprite mining district was recorded on August 1, 2001. The 30-m resolution SWIR bands were spatially registered to the 15-m resolution VNIR bands, thereby forming a nine-band image data set. A subset corresponding to the Cuprite mining district and to the coverage of the 1997 AVIRIS data was derived from the ASTER scene. Using similar analytical procedures, we compared the ASTER and AVIRIS mapping results.

Data calibration

The pixels comprising an airborne or satellite image are records of the energy reflected from the surface into each spectral band, whether it is the nine ASTER VNIR and SWIR

method in which laboratory spectra resampled to ASTER bandpasses, instead of ASTER image spectra, were used proved to be less effective. Differences between the image spectra and laboratory spectra are attributed to imperfections in the calibration and to local image variations related to optical and electronic quality of the ASTER data (Iwasaki, et al., 2002).

Eight spectral end members were identified from the corrected ASTER image spectra (Fig. 6). These eight image spectra were used as reference in a matched-filtering procedure (Harasanyi and Chang, 1994). This procedure minimizes the response of the background materials by projecting each pixel vector onto a subspace that is orthogonal to the background spectra, and then maximizes the response of the end members of interest by comparing the residual pixels to each of the reference spectra (Fig. 6). ASTER bands five through nine were used for all the end members because of the concentration of spectral absorption features in the 2.1 to 2.45 μm wavelength region, except the unaltererd tuff and chlorite + muscovite end members, for which all nine bands were used.

In each of the resulting matched-filter images the degree of match is indicated by linearly scaled digital numbers (DN), with higher numbers representing good matches and vice versa. Pixels corresponding to the highest degree of match for each end member were transferred digitally to the ASTER band 1 image and assigned a color (Fig. 7A). Determination of the DN range to represent each end member was based on
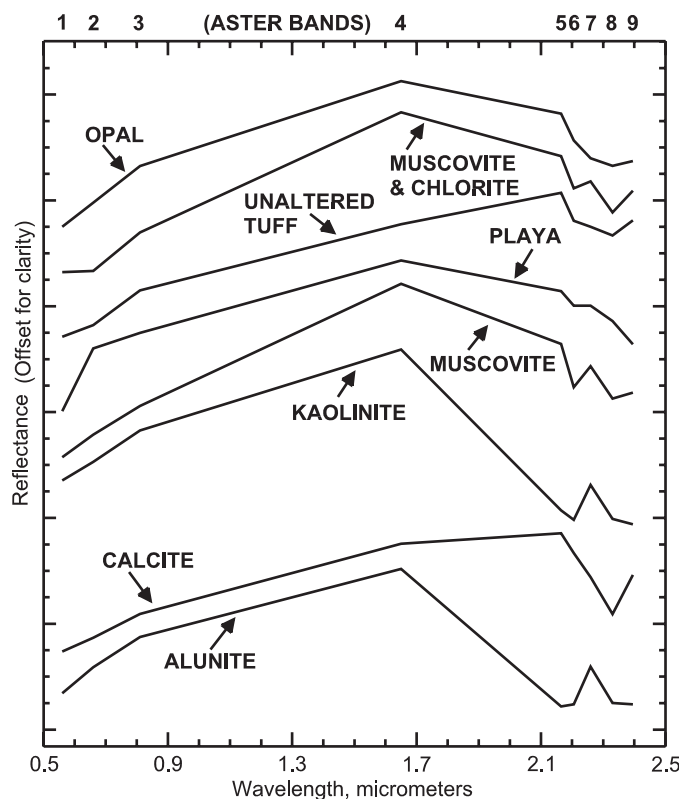
the coherence of the spatial distribution and the lack of widely scattered pixels. Previous spectral reflectance studies conducted in the Cuprite district, particularly in situ measurements and AVIRIS data analysis, also aided in selecting the DN ranges for these end members (Abrams et al., 1977; Ashley and Abrams, 1980; Swayze, 1997; Swayze et al., 1998).

The ASTER results show general agreement with the mapped distribution of the hydrothermally altered rocks (Fig. 3). The mapped opal end member corresponds to the silicified core in the eastern part due to the abundance of hydrothermal quartz (red, Fig. 3; purple, Fig. 7A), which exhibits a broad Si-O-H absorption feature centered near 2.3 μm (opal, Fig. 6). Alunite and kaolinite are the spectrally dominant minerals in the opalized map unit (red and green, respectively, Fig. 7A). Kaolinite corresponds to the narrow zone of argillized rocks in the eastern part and, locally, to similar exposures in the western part (green, Fig. 7A; yellow, Fig. 3).

Five spectral end members correspond to the country rocks and playa deposit within the mining district. The calcite end member is generally restricted to the area underlain by the Mule Spring Limestone and Emigrant Formation in the western part of the district (Fig. 2; blue, Fig. 7A). The distribution of the muscovite end member pixels appears to be consistent with the occurrence of the Harkless Formation siltstone and associated colluvial material (Fig. 2; cyan, Fig. 7A). The muscovite + chlorite end member is limited to the western margin of the hydrothermally altered rocks west of U.S. Highway 95 (Fig. 3; yellow, Fig. 7A), where chloritic phyllite of the Harkless Formation is exposed (written commun., G. Swayze, 2002) . The unaltered tuff end member exhibits a weak broad absorption feature in the 2.20–2.33 μm wavelength region, which we attribute to a combination of vitrophyric materials and clayey weathering products (unaltered tuff, Fig. 6). This weak absorption feature and the low slope of the spectrum distinguish the unaltered tuff from the other spectral end members (lavender, Fig. 7A). The playa deposit reflectance spectrum displays a weak absorption feature centered in the 2.20 μm region and is represented by dark green in Figure 7A.

AVIRIS data analysis

Selection of 11 end members was based on the results of pixel-purity index processing of an AVIRIS image subset, which approximates the ASTER subset coverage (Figs. 7A and B). The end member spectra are shown in two categories: (1) hydrothermally altered rocks, and (2) country rocks (Figs. 8A and B, respectively). These spectra were used as references in matched filter processing in the 2.00- to 2.45-μm region of the AVIRIS data.

Comparison of the AVIRIS and ASTER matched-filter results indicate good agreement, although dickite, buddingtonite, and the hydrothermal illite were mapped only in the AVIRIS image (orange, aquamarine, and pink, respectively; Fig. 7B). Mapping these minerals is important for characterizing the hydrothermally altered rocks in the district, but the ASTER instrument spectral resolution is not adequate to distinguish the subtle spectral differences between dickite and alunite, and dickite and kaolinite.
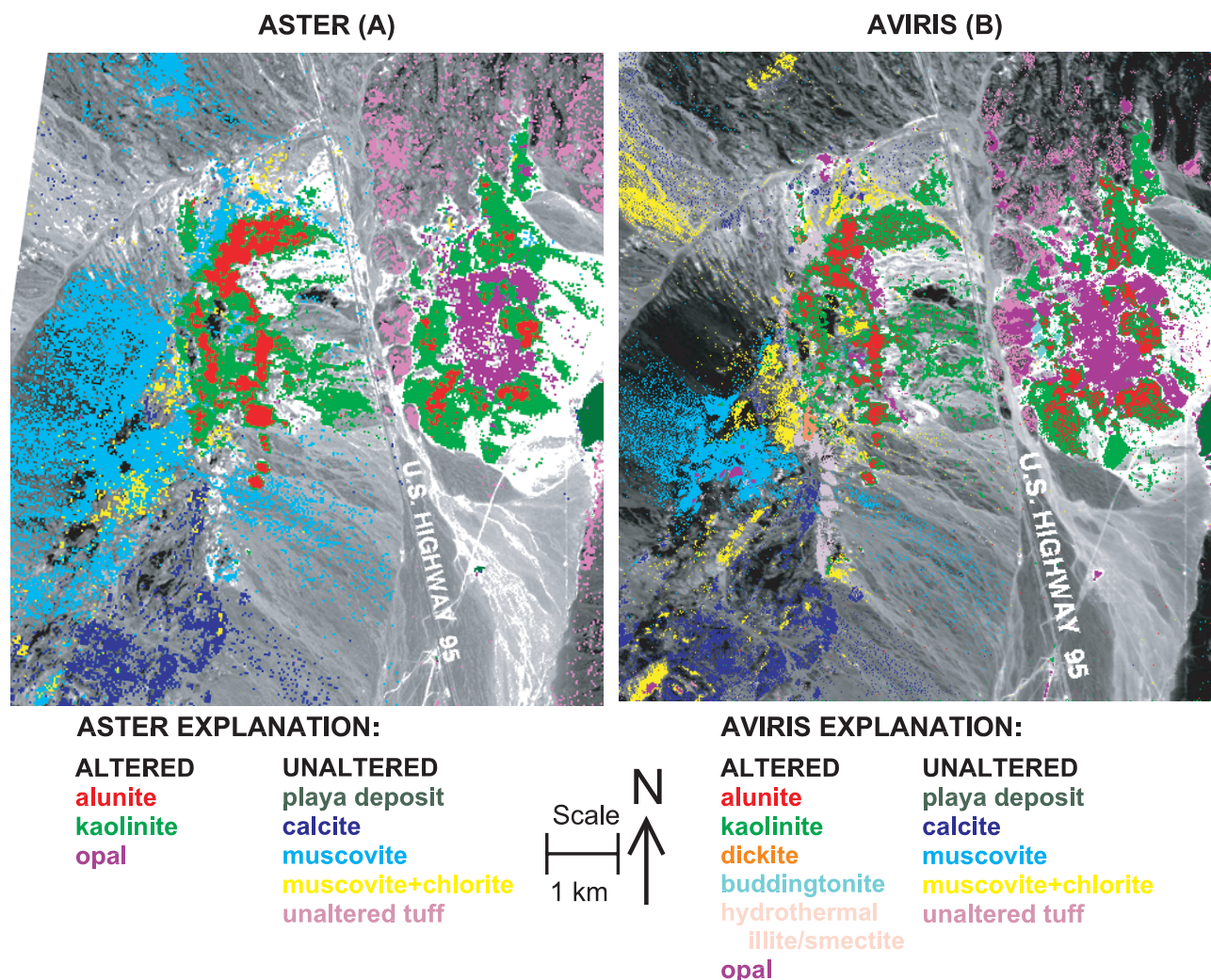

FIG. 6.   ASTER image spectra of the lithologic spectral end members mapped in the Cuprite mining district, Nevada.

ASTER (A)

AVIRIS (B)

ASTER EXPLANATION:

ALTERED	UNALTERED
alunite	playa deposit
kaolinite	calcite
opal	muscovite
	muscovite+chlorite
	unaltered tuff

Scale

N

1 km

AVIRIS EXPLANATION:

ALTERED	UNALTERED
alunite	playa deposit
kaolinite	calcite
dickite	muscovite
buddingtonite	muscovite+chlorite
hydrothermal illite/smectite	unaltered tuff
opal	

FIG. 7. Results of matched-filter processing based on image spectra representing lithologic spectral end members overlain on base image: A, ASTER band 1 base image; B, AVIRIS band 25 base image.

Identifying the hydrothermal illite in the AVIRIS image is the basis for mapping the altered quartz latite dike (Figs. 2 and 3; pink, Fig. 7B), but this end member is incorporated in the ASTER muscovite category and, hence, the altered dike is not mapped in the ASTER image (Fig. 7A).

Summary

This evaluation of ASTER data shows that subtle spectral reflectance differences recorded in the VNIR-SWIR wavelength region can be used as a basis for mapping the surface distribution of certain individual minerals and mineral groups, and hence to delineate hydrothermal alteration zones. In the intensely leached rocks of the silicified zone, opal is the spectrally dominant mineral; whereas, in the opaline alteration zone, alunite and kaolinite are the spectrally dominant minerals (Figs. 3 and 7A). In addition, the distribution of unaltered country rock units was generally mapped in the ASTER image data because of the presence of spectrally dominant calcite in the Mule Spring Limestone and Emigrant Fm. exposures, muscovite in the Harkless Fm. rocks, and the

relatively flat spectra of the tuffaceous rocks and playa deposits with weak absorption features at 2.20, and at 2.33 and 2.20 μm, respectively (Figs. 2 and 7A).

Analysis of the high spectral resolution AVIRIS data of the Cuprite district permits identification and mapping of several individual minerals, including dickite, buddingtonite, and hydrothermal illite, which were not identified in the ASTER data analysis. This mineralogical information is important for determining the formative conditions within the hydrothermal system. However, the availability of AVIRIS and spectrally similar airborne data is very limited compared to the ASTER coverage, which is nearly complete for the land surface. Landsat Thematic Mapper (TM) data, which have similar spatial resolution and very extensive coverage, records reflected radiation in four VNIR and two SWIR bands (Fig. 9). Although TM data have proven very useful for discriminating lithologies in well-exposed areas, limonite is the only mineralogical category that can be identified consistently (Goetz et al., 1983). Hydrothermally altered rocks are commonly distinctive in TM images because of absorption in the 2.20-μm
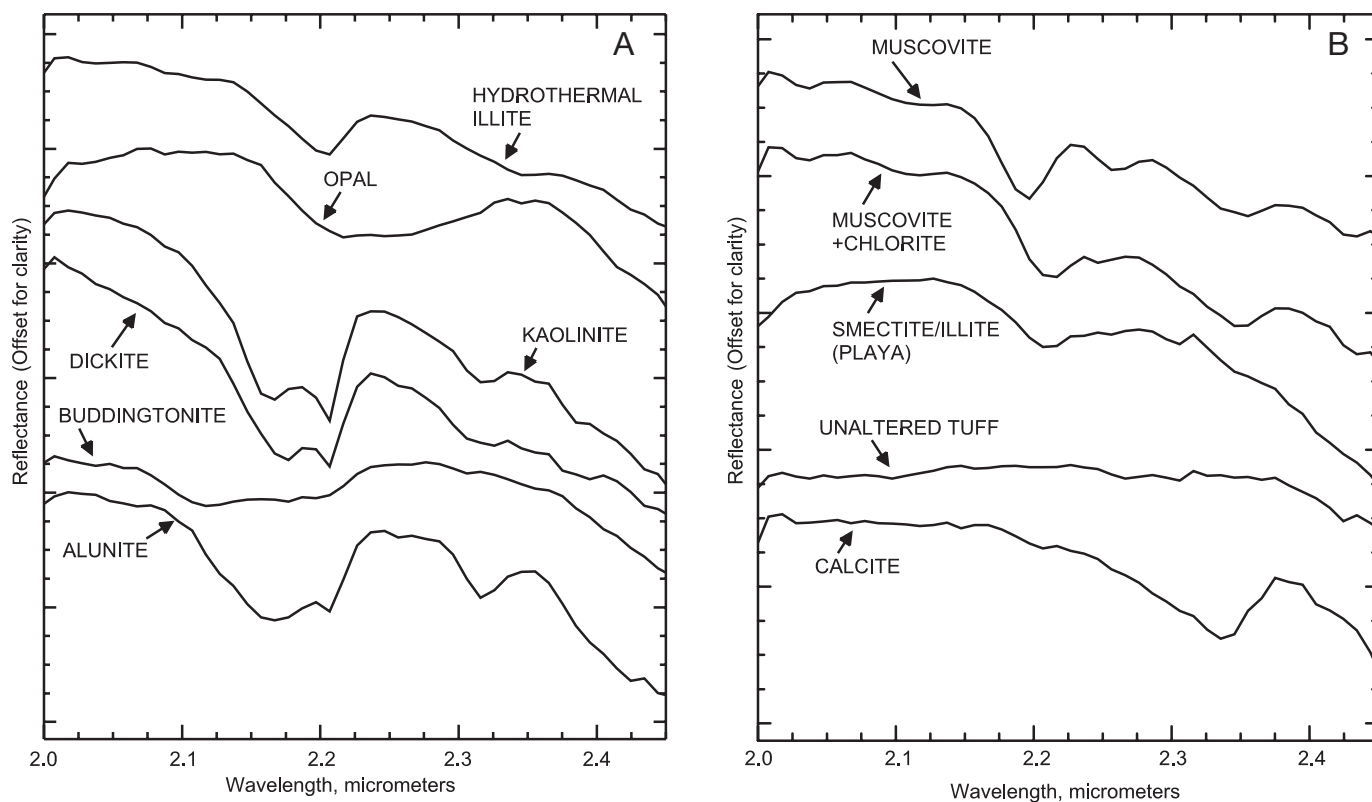
FIG. 8. AVIRIS image spectra of selected spectral end members: A. hydrothermally altered rocks; and B. country rocks.
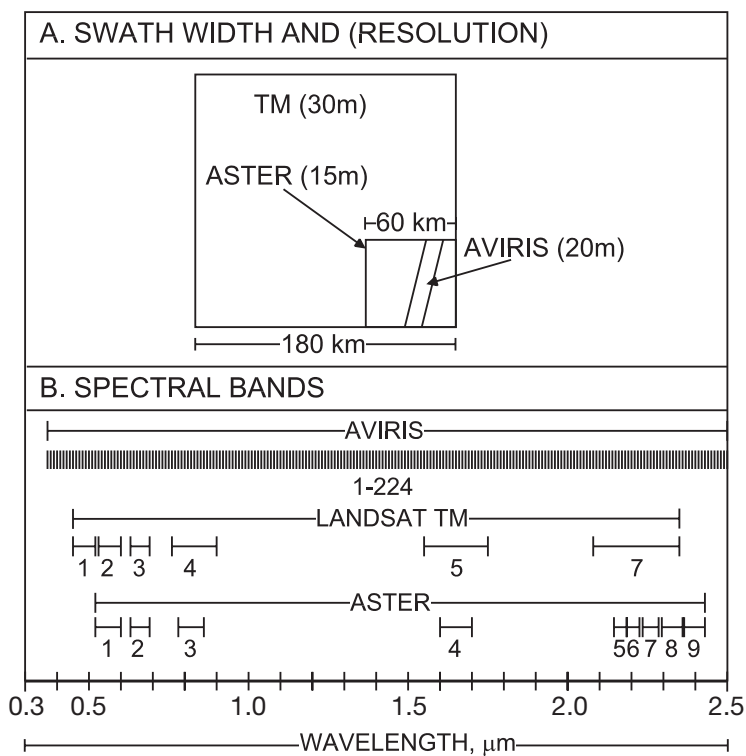

FIG. 9. Comparison of ASTER, AVIRIS, and Landsat Thematic Mapper (TM) VNIR and SWIR image spatial and spectral characteristics: A, Swath width and (spatial resolution). Landsat TM 5 and 7 have 30-m resolution in six VNIR and SWIR bands, and TM 7 has 15-m resolution in a single panchromatic band. ASTER VNIR resolution is 15 m, and the SWIR resolution is 30 m. AVIRIS high-altitude data have 20-m resolution within 11-km wide swaths, and 5-m resolution data can be acquired at low altitude for 2.5-km wide strips. B, Spectral bands.

band due to the presence of O-H minerals, but diminished reflectance in this band can also be related to carbonate minerals and water in soil and plants. VNIR and SWIR ASTER data analysis overcomes most of these ambiguities, thereby improving the quality of the remotely derived lithologic maps and reducing the time and cost required for field evaluation.

Acknowledgments

May 1, 2002; February 3, 2003

REFERENCES

Abrams, M.J., Ashley, R.P., Rowan, L.C., Goetz, A.F.H., and Kahle, A.B., 1977, Mapping of hydrothermal alteration in Cuprite mining district, Nevada, using aircraft scanner images for the spectral region 0.46 to 2.34 mm: Geology, v. 5, p. 713–718.

Abrams, M.J., Brown, D., Lepley, L., and Sadowski, R, 1983, Remote sensing of porphyry copper deposits in Southern Arizona: ECONOMIC GEOLOGY, v. 78, p. 591–604.

Albers, J.P., and Stewart, J.H., 1972, Geology and mineral deposits of Esmeralda County, Nevada: Nevada Bureau of Mines and Geology Bulletin, v. 78, 80 p.

Ashley, R.P., and Abrams, M.J., 1980, Alteration mapping using multispectral images—Cuprite mining district, Esmeralda County, Nevada: U.S. Geological Survey Open-File Report 80-367, 17 p.

Boardman, J.W., Kruse, F.A., and Green, R.O., 1995, Mapping target signatures via partial unmixing of AVIRIS data: Proceedings of the Fifth JPL Airborne Earth Science Workshop, Jet Propulsion Laboratory, Pasadena, California, January 23–26, 1995, JPL Publication 95-01, p. 23–26.

Clark, R.N., Swayze, G.A., and Heidebrecht, K., 1995, Calibration to surface of terrestrial imaging spectrometer data: Comparison of methods, *in* R. O. Green, R.O., ed., Summaries of the Fifth Annual JPL Airborne Earth Science Workshop: AVIRIS Workshop, Jet Propulsion Laboratory, Pasadena, California, January 23–26, 1995, JPL Publication 95-1, v. 1, p. 41–42.

Cocks, T., Jenssen, R., Stewart, A., Wilson, I., and Shields, T., 1998, The HyMap airborne hyperspectral sensor: The system, calibration and performance: 1st EARSel (European Association of Remote Sensing Laboratories) Workshop on Imaging Spectroscopy, Zurich, EARSel, Proceedings, p. 37–43.

Crowley, J. K., Rowan, L., Podwysocki, M., 1988, Evaluation of airborne/infrared imaging spectrometer data of the Mountain Pass, California Carbonatite complex, *in* Vane, G., ed., Proceedings of the Airborne Visible/Infrared Imaging Spectrometer (AVIRIS) Performance Evaluation Workshop: Jet Propulsion Laboratory, Pasadena, California, June 6–8, 1988, JPL Publication 88-38, p. 155–161.

Fujisada, H., 1995, Design and performance of ASTER instrument, *in* Fujisada, H., and Sweeting, M.N., eds., Proceedings SPIE (International Society for Optical Engineering), v. 2583, p. 16–25.

Goetz, A.F.H., and Srivastava, V., 1985, Mineralogical mapping in the Cuprite mining district, Nevada, *in* Vane, G., and Goetz, A.F.H., eds., Proceedings of the Airborne Imaging Spectrometer Workshop: Jet Propulsion Laboratory, Pasadena, California, April 8–10, 1985, JPL Publication 85-41, p. 22–31.

Goetz, A.F.H., Rock, B.N., and Rowan, L.C., 1983, Remote sensing for exploration: An overview: ECONOMIC GEOLOGY, v. 78, p. 573–590.

Green, R.O., 1991, Retrieval of reflectance from AVIRIS radiance using a radiative transfer code, *in* Green, R.O, ed., Proceedings of the Third AVIRIS Workshop: Jet Propulsion Laboratory Pasadena, California, May 20–21, JPL Publication 91-28, p. 200–210.

Harsanyi, J.C., and Chang, C., 1994, Hyperspectral image classification and dimensionality reduction: An orthogonal subspace projection approach: IEEE Transactions Geoscience Remote Sensing, v. 32, p. 770–785.

Hausback, B.P., Deino, A.L., Turrin, B.T., Mckee, E.H., Frizzell,V. A., Jr., Noble, D.C., and Weiss, S.I., 1990, New ^{40}Ar/^{39}Ar ages for the Spearhead and Civet Cat Canyon Members of the Stonewall Flat Tuff, Nye County, Nevada—evidence for systematic errors in standard K-Ar Determinations on sanidine: Isochron/West, no. 56, p. 3–7.

Hook, S., Elvidge, C.D., Rast, M., and Watanabe, H., 1991, An evaluation of mineral absorption features in short wave infrared (SWIR) data from the AVIRIS and GEOSCAN instruments at Cuprite, Nevada: Geophysics, v. 56, , p. 1432–1440.

Hunt, G.R., 1977, Spectral signatures of particulate minerals in the visible and near infrared, Geophysics, v. 42, p. 501–513.

Iwasaki, A., Fujisada, H., Akao, H., Shindou, O., and Akagi, S., 2002, Enhancement of spectral separation performance of ASTER/SWIR, *in* Strojnik, M. and Andresen, B., eds., Proceedings SPIE (International Society for Optical Engineering), Infrared Spaceborne Remote Sensing IX: San Diego, California, July 29–Aug. 3, 2001, SPIE, v. 4486, p. 42–50.

Kruse, F.A., Kierein-Young, K.S., and J.W. Boardman, 1990, Mineral mapping at Cuprite, Nevada, with a 63-channel imaging spectrometer: Photogrammetric Engineering and Remote Sensing, v. 56, p. 83–92.

Kruse, F.A., Lefkoff, A. B., Boardman, J.B., Heidebreicht, K.B., Shapiro, A.T., Barloon, P.J., and Goetz, A.F.H., 1993, The Spectral Image Processing System (SIPS)—interactive visualization and analysis of imaging spectrometer data, Remote Sensing of Environment, v. 44, p. 145–163.

Myers, C.A., and Hemley, J.J., 1967, Wall-rock alteration, *in* Barnes, H.L., ed., Geochemistry of hydrothermal ore deposits: New York, Holt, Rinehart and Winston, Inc., p. 167–232.

Podwysocki, M.H., Segal. D.B., and Abrams, M.J., 1983, Use of multispectral images for assessment of hydrothermal alteration in the Marysvale, Utah, mining area: ECONOMIC GEOLOGY, v. 78, p. 675–687.

Rast, M., Hook, S., Elvidge, C.D., and Alley, R.B., 1991, An evaluation of techniques for the extraction of mineral absorption features from high spectral resolution remote sensing data: Photogrammetric Engineering and Remote Sensing, v. 57, p. 1303–1309.

Rowan, L.C., and Mars, J.C., 2003, Lithologic mapping in the Mountain Pass, California, area using Advanced Spaceborne Emission and Reflection Radiometer (ASTER) data: Remote Sensing of Environment, v. 82, p. 350–366.

Rowan, L.C., Wetlaufer, P.H., Goetz, A.F.H., Billingsley, F.C., and Stewart, J.H., 1974, Discrimination of rock types and detection of hydrothermally altered areas in south-central Nevada: U.S. Geological Survey Professional Paper 883, 35 p.

Rowan, L.C., Goetz, A.F.H., and Ashley, R.P., 1977, Discrimination of hydrothermally altered rocks and unaltered rocks in visible and near infrared multispectral images: Geophysics, v. 42, p. 522–535.

Swayze, G.A., 1997, The hydrothermal and structural history of the Cuprite mining district, southwestern Nevada: An integrated geological and geophysical approach: Ph.D. dissertation, Boulder, Colorado, University of Colorado, 399 p.

Swayze, G.A., Clark, R.N., Kruse, F., and Sutley, S., 1992, Ground-truthing AVIRIS mineral mapping at Cuprite, Nevada, *in* Green, R.O, ed., Summaries of the Third Annual JPL Airborne Geoscience Workshop: Jet Propulsion Laboratory, Pasadena, California, June 1–5, 1992, JPL Publication 92-14, v. 1, p. 47–49.

Swayze, G.A., Clark, R.N., Goetz, A.F.H., Livo, K.E., and Sutley, S.S., 1998, Using imaging spectroscopy to better understand the hydrothermal and tectonic history of the Cuprite mining district, Nevada, *in* Green, R.O., ed., Summaries of the Seventh JPL Airborne Earth Science Workshop: Vol. 1, 1998: Jet Propulsion Laboratory, Pasadena, California, January 12–16, 1998, JPL Publication 97-21, p. 383–384.

Weiss, S.I., and Noble, D.C., 1989, Stonewall Mountain volcanic center, southern Nevada: Stratigraphic, structural, and facies relations of outflow sheets, near-vent tuffs, and intracaldera units: Journal Geophysical Research, v. 94, no. B5, p. 6059–6072.